A Theoretical Analysis of Quantum Noise in Semiconductor Lasers Operating with Self-Sustained Pulsation

IEICE TRANS. ELECTRON., VOL. E81–C, NO. 2 FEBRUARY 1998

PAPER

A Theoretical Analysis of Quantum Noise in Semiconductor Lasers Operating with Self-Sustained Pulsation

Minoru YAMADA[†a)], *Member*

SUMMARY The semiconductor lasers operating with self-sustained pulsation are under developing to be lasers which are less disturbed by the optical feedback from a surface of optical disk. Structures setting saturable absorbing regions utilizing the multi-layer configuration become popularly used for giving stronger pulsation. However, the quantum (intensity) noise in these lasers tends to be enhanced. The ridge stripe structure, of which almost self-sustained pulsation lasers consist, seems to give a leak current flowing along plane of the cladding region. Such leak current also increases the quantum noise. In this paper, theoretical calculations of operating characteristics, such as the self-sustained pulsation, the optical output, the quantum noise as well as the transverse filed profile, are theoretically analyzed by including the above mentioned several phenomena.

key words: *semiconductor laser, quantum noise, self-sustained pulsation, transverse mode, saturable absorbing region*

1. Introduction

Generation of the optical feedback induced noise in the semiconductor laser is a terrible problem for development of the optical disk system. The phenomenon of the self-sustained pulsation in the laser has been found to be effective for the reduction of the feedback noise [1]–[3]. Urgent improvements getting stronger pulsation have been tried [4]–[7]. Setting an additional saturable absorbing (SA) region in the upper to the active region is a method of the improvements. However, lasers having such additional SA region tend to show rather higher quantum (intensity) noise [8], [9] especially in the low power operation, which corresponds to the reading state in the magneto-optical disk system.

On the other hand, these lasers giving stronger self-pulsation tend to show a rather high threshold current level. One intrinsic reason of the increase of the threshold current the increase of the optical absorption by the added SA region. However, the obtained threshold current level in real devices seems much higher than the value expected by taking into account the increased optical absorption. Another possible reason of the high threshold current may be laid on the existence of a leak current flowing in the lateral width direction along a cladding region located beneath the current blocking region in the ridge stripe structure, which is the most typical stripe structure to get the self-sustained pulsation. The leak current, in general, raises both the threshold current and the quantum noise.

In this paper, theoretical calculations of the operating characteristics of the self-sustained pulsation lasers, such as strength of the pulsation, output power level, quantum noise, and profiles of the transverse mode, are presented. The mode competition phenomena and the effect of the optical feedback are, however, not treated in this paper.

2. Model of Analysis

A crosssectional model of the laser for this analysis is shown in Fig. 1. The material system of $Al_xGa_{1-x}As$ is supposed in the numerical calculations. Abbreviated notations and the material type of these regions are as follows: Act. is the active region made of the intrinsic-type material formed by the double hetero (DH) structure or the multi quantum well (MQW) structure. S.A. is the saturable absorbing (SA) region of the p-type material formed by the DH or MQW structure. Cu.Bl. is the current blocking region of the n-type material. Cap is the cap region of the p-type material to transfer the

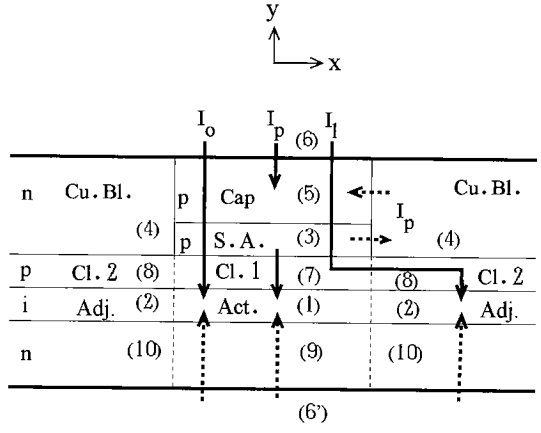

Fig. 1 Crosssectional view of the self-sustained pulsation laser. Act. is the active region, S.A. is the saturable absorbing region, Cu.Bl. is the current blocking region, Cap is the cap region and Adj. is an adjoining region to the active region. All regions are also numbered.

Manuscript received August 4, 1997.
Manuscript revised October 22, 1997.

[†]The author is with the Faculty of Engineering, Kanazawa University, Kanazawa-shi, 920–8667 Japan.
a) E-mail: myamada@t.kanazawa-u.ac.jp

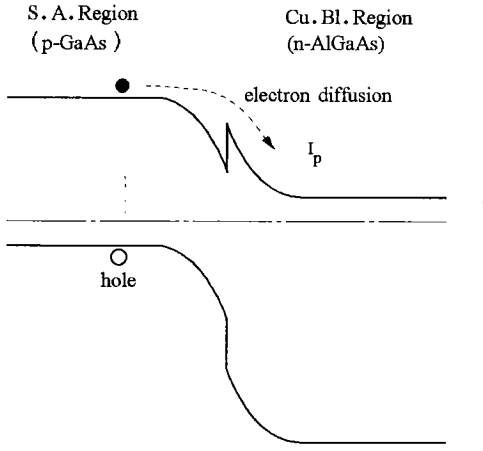

Fig. 2 Electron diffusion from S.A. to Cu.Bl. regions. Absorbed electron in the S.A. region diffuse into the Cu.Bl. region, resulting in the hole re-injection from the S.A. region to the Act. region.

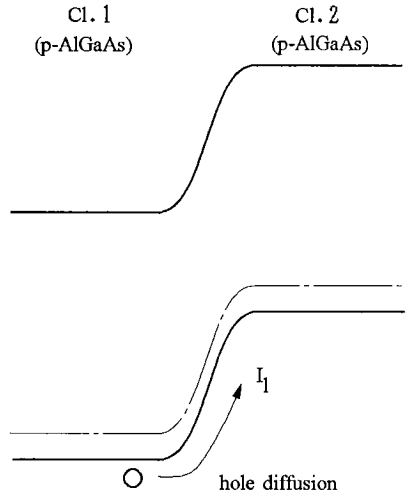

Fig. 3 Hole diffusion from Cl.1 to Cl.2 regions. Holes in the Cl.1 region diffuse into the Cl.2 region and may recombine in the Adj. region.

holes from the electrode. Adj. is an adjoining region in the lateral (x) direction to the active region. The Adj. regions work as saturable absorbing regions when the optical field spread sufficiently into these regions as the case of the gain guiding property [3], [4], but are quiet when the field is more confined in the active region by the index guiding property. Flows of holes and electrons are indicated by arrows with solid lines and dotted lines, respectively. I_o is the original driving current flowing into the active region. Existence of additional current components of I_p and I_l are claimed as in the following discussions.

Pairs of electrons and holes are generated in the S.A. region by optical absorption. Electrons of the generated pairs diffuse into the n-type Cu.Bl. regions and recombine with holes in the Cu.Bl. regions or the p-type Cap region, forming a current component of I_p as illustrated in Fig. 2, where the chain line indicates the Fermi level. The generated holes in the S.A. region have to be injected into the active region to keep the electrical neutral condition in the S.A. region. This hole injection may be called the photon recycling effect. The effects of the diffusion and the photon recycling enhance the self-sustained pulsation, because the generated electron-hole pairs decay rapidly.

The injected holes from the p-side electrode can flow along the Cl.2 region beneath the Cu.Bl. region in the lateral (x) direction as illustrated in Fig. 3, and re-combine with the electrons at far positions from the Act. region. This effect forms the current component I_l of Fig. 1.

The total injection current I at the electrode is then given by

$$I = I_o + I_p + I_l \,. \tag{1}$$

3. Dynamic Equations

Each region in Fig. 1 is numbered with an integer i or j. The electrodes are also counted as geometrical regions in this analysis. The injected carrier density n_i is defined as an averaged value of the increased density of the electrons and the holes from the thermal equilibrium state in the i-th region as

$$n_i = (n_{electron} - \tilde{n}_{electron} + n_{hole} - \tilde{n}_{hole})/2 \tag{2}$$

where, $n_{electron}$ and n_{hole} are the densities of the existing electrons and holes, respectively, and $\tilde{n}_{electron}$ and $\tilde{n}_{hole}$ are the densities of the electrons and the holes at the thermal equilibrium state, respectively. Corresponding to this injected carrier density, the injected carrier number N_i is defined with the effective volume V_i

$$N_i = n_i V_i \,. \tag{3}$$

For the calculation of the noise, formulation with the injected carrier number N_i is more fundamental than that with the injected carrier density n_i, because the noise comes from fluctuations on the quantum numbers rather than on the spatial densities. Furthermore the effective volume V_i is not constant for the time variation under pulsing operation in our model.

Basing on a simplified treatment as in Refs. [3], [4], variations of the photon number S and the injected carrier number N_i are formulated as

$$\frac{dS}{dt} = \left[\sum_i a_i \xi_i (N_i - N_{gi})/V_i - BS - G_{th}\right] S + M \sum_i a_i \xi_i N_i / V_i + F(t) \tag{4}$$

$$\frac{dN_i}{dt} = -a_i \xi_i (N_i - N_{gi}) S / V_i - N_i / \tau_{si}$$

$$+\sum_{j\neq i}\{N_j/T_{ji} - N_i/T_{ij} + (I_{ji} - I_{ij})/e\}$$

$$+ Q_i(t) \tag{5}$$

where, a_i is the differential gain coefficient defined on characteristics of the linear gain versus the injected carrier density, ξ_i is the field confinement ratio in the transverse cross-section, N_{gi} is the transparent carrier number, B is the gain saturation coefficient, G_{th} is the threshold gain level, τ_{si} is the carrier life-time, T_{ij} is an equivalent life-time giving the carrier diffusion from i to j regions, I_{ji} gives carrier injection from j to i regions and M is an equivalent total number of the longitudinal modes. It should be noted here that almost all coefficients in Eqs. (4) and (5) (other than e, M and G_{th}) vary with the time through variation of the carrier number under pulsing operation.

Let us mention here the used assumptions and model to determine the parameters introdued in Eqs. (4) and (5) [3], [4]. The field distribution function in each region is assumed to be sinusoidal or exponential for x and y directions with complex propagation constant γ_i. As the width or the thickness of the external open regions (such as the Adj., the Cu.Bl and the Cap regions), the larger value of the carrier diffusion length of $\sqrt{D_c\tau_{si}}$ or the field extending range of $1/Re\gamma_i$ is picked up, where D_c is the carrier diffusion constant. When the region consists with two areas as in the left and the right sides in Fig. 1, a doubled value of thus obtained length should be substituted as the width W_i or the thickness d_i to represent the two areas at the same time. Of course, the initially set length of W_i and d_i should be substituted when boundaries of the i-th region were well defined. Then we can determine the volume of the i-th region as [4]

$$V_i = W_i d_i L \tag{6}$$

where, L is length of the laser. The spatial carrier distribution is regarded to be almost uniform within this volume [4].

The transparent carrier number N_{gi} is given with the transparent carrier density n_{gi} which is a material constant as

$$N_{gi} = n_{gi} V_i \,. \tag{7}$$

The threshold gain level is given with the refractive index n_{ro}, the loss coefficient κ and the power reflectivities R_f and R_b at the front and the back facets, respectively:

$$G_{th} = \frac{c}{n_{ro}}\left(\kappa + \frac{1}{2L}\ln\frac{1}{R_f R_b}\right) \tag{8}$$

The carrier life time τ_{si} in the direct transition material (that is, the aluminum concentration x is less than 0.35) is given with a proportional constant A_s and the injected carrier number as

$$\tau_{si} = V_i/(A_s N_i) \,. \tag{9}$$

The saturation coefficient B is given with the dipole moment R_{cv}, the intraband relaxation time τ_{in} and other parameters in the Act. ($i = 1$) region as [3]

$$B = \frac{9\hbar\omega}{4\epsilon_o n_r^2}\left(\frac{\tau_{in}}{\hbar}\right)^2 \frac{R_{cv}^2 a_1 \xi_1^2 (N_1 - N_{g1})}{V_1^2} \,. \tag{10}$$

The equivalent carrier lifetime T_{ij} for spatial diffusion from the internal bounded region i (Act. or S.A.) to the external open region j (Adj. or Cu.Bl.) which is located at both sides in the lateral (x) direction is characterized with the stripe width W_i and the diffusion constant D_c as [4]

$$T_{ij} = W_i^2/(2D_c\, f_{ij}) \tag{11}$$

and for the counter diffusion from the external region j to the internal i as

$$T_{ji} = V_j T_{ij} f_{ij}/(V_i\, f_{ji}) \tag{12}$$

where, f_{ij} and f_{ji} are factors having values of $0 \sim 1$ to count less effective diffusion caused by the single type of carrier (either the electron or the hole) not by the ambipolar (a pair of the electron and the hole), because the Coulomb force between the electron and the hole prevents the diffusion.

The equivalent total number of the longitudinal modes is evaluated with the half angular frequency width of the linear gain $\Delta\omega$ as [10]

$$M = \Delta\omega\, n_r L/2c \,. \tag{13}$$

The added terms $F(t)$ and $Q_i(t)$ in Eqs. (4) and (5) are the Langevin noise sources associated with the photon emission or the electron transition and are expanded into frequency components:

$$F(t) = \int F_\Omega e^{j\Omega t} d\Omega \tag{14}$$

$$Q_i(t) = \int Q_{i\Omega} e^{j\Omega t} d\Omega \tag{15}$$

The magnitude of the frequency components F_Ω and $Q_{i\Omega}$ are given by DC terms as in the next equations, since the fluctuation forms a Poisson's distribution profile where the amount of the dispersion is the same as the averaged value:

$$\langle F_\Omega^2\rangle = \int F(t)F(t+\tau)e^{j\Omega\tau}d\tau$$
$$= 2\sum_i \overline{a_i \xi_i N_i (S+M)/V_i} \tag{16}$$

where, $\bar{}$ indicates taking a timely averaged value as a DC component.

We should be careful in evaluating the carrier injection. The term I_{ji} is defined for the carrier injection

not for the current injection in more exact discussion. When the carrier is the electron, flowing direction of the current is inverse to that of the injected carrier. I_{ji} is defined as the difference of two components k_{ji} and k_{ij},

$$I_{ji} = k_{ji} - k_{ij} \tag{17}$$

where, k_{ji} is a flow component caused by a source in the j-th region while k_{ij} is another component caused by another source in the i-th region. There is no restricted relation between these components which generally satisfy $k_{ji} \neq -k_{ij}$, although the resulted carrier injection should have a relation of $I_{ji} = -I_{ij}$ because of the continuity of the carrier number. An example is the hole injection from the p-side electrode ($j = 6$) to the cap region ($i = 5$). That is $k_{65} = I$ while $k_{56} = 0$.

The magnitude of the fluctuation on the carrier number is given with the summed value of these transition and flow components. Then

$$\langle Q_{i\Omega}^2 \rangle = 2\left\{\overline{a_i\xi_i N_i S/V_i} + \overline{N_i/\tau_{si}} + \sum_{j\neq i}\overline{N_i/T_{ij}} + \sum_{j\neq i}(k_{ji} + k_{ij})/e\right\} \tag{18}$$

is obtained.

Mutual correlations among variations of the photon and the carrier numbers are given by

$$\langle F_\Omega Q_{i\Omega}\rangle = -\overline{a_i\xi_i(N_i S + N_{gi}S + MN_i)/V_i} \tag{19}$$

and

$$\langle Q_{i\Omega}Q_{j\Omega}\rangle = -\left\{\overline{N_i/T_{ij}} + \overline{N_j/T_{ji}} + 2(k_{ij} + k_{ji})/e\right\} \tag{20}$$

The photon number and the carrier number are re-written with deterministic components noted by $\hat{}$ and fluctuated components noted by Ω

$$S = \hat{S} + \int S_\Omega e^{j\Omega t}d\Omega \tag{21}$$

$$N_i = \hat{N}_i + \int N_{i\Omega}e^{j\Omega t}d\Omega\,. \tag{22}$$

Since some components I_{ji} of the carrier injection are related to the carrier diffusion, these components also should be re-written with the deterministic and the fluctuated terms as

$$I_{ji} = \hat{I}_{ji} + \int I_{ji\Omega}e^{j\Omega t}d\Omega\,. \tag{23}$$

The dynamic equations of the deterministic components are obtained from Eqs. (4) and (5) by neglecting the fluctuated components, because the later components are much smaller than the former ones.

$$\frac{d\hat{S}}{dt} = \left[\sum_i a_i\xi_i(\hat{N}_i - N_{gi})/V_i - B\hat{S} - G_{th}\right]\hat{S} + M\sum_i a_i\xi_i\hat{N}_i/V_i \tag{24}$$

$$\frac{d\hat{N}_i}{dt} = -a_i\xi_i(\hat{N}_i - N_{gi})\hat{S}/V_i - \hat{N}_i/\tau_{si} + \sum_{j\neq i}\{\hat{N}_j/T_{ji} - \hat{N}_i/T_{ij} + (\hat{I}_{ji} - \hat{I}_{ij})/e\} \tag{25}$$

The equations of the fluctuated components are obtained by multiplying $\exp[-j\Omega t]$ to Eqs. (4) and (5) and taking the time average. Coefficients of the fluctuated components are given by timely averaged values noted by $\bar{}$, such that

$$\left\{j\Omega + G_{th} + 2\overline{BS} - \sum_i\overline{a_i\xi_i(N_i - N_{gi})/V_i}\right\}S_\Omega - \sum_i(\overline{a_i\xi_i(S + M)/V_i})N_{i\Omega} = F_\Omega \tag{26}$$

and

$$\overline{a_i\xi_i(N_i - N_{gi})/V_i}\,S_\Omega + \{j\Omega + \overline{1/\tau_{si}} + \overline{a_i\xi_i S_i/V_i} + \sum_{j\neq i}\overline{1/T_{ij}})N_{i\Omega} - \sum_{j\neq i}(\overline{(1/T_{ji})}\}N_{j\Omega} - \sum_{j\neq i}(I_{ji\Omega} - I_{ij\Omega})/e = Q_{i\Omega} \tag{27}$$

The fluctuated components of the current $I_{ji\Omega}$ and $I_{ij\Omega}$ are characterized with each injection mechanism, where some of them are functions of the fluctuated carrier number and others are put zero when the laser is driven with a constant DC current source.

The fluctuated components S_Ω and $N_{i\Omega}$ are then obtained as solutions of Eqs. (26) and (27) with several DC values which are examined by numerical analysis of the dynamic equations Eqs. (24) and (25).

The value of the relative intensity noise (RIN) is obtained by the next equation:

$$RIN = \langle {S_\Omega}^2\rangle/\overline{S}^2 \tag{28}$$

The output power P_{out} from the front facet is given by

$$P_{out} = \frac{(1 - R_f)\pi c^2\hbar\overline{S}}{n_{ro}\lambda_o L} \times \frac{\ln(1/R_f R_b)}{(1 + \sqrt{R_f/R_b})(1 - \sqrt{R_f R_b})} \tag{29}$$

where, λ_o is the central wavelength of the laser.

4. Parameter Settings in a Specified Model

The assumed geometrical and material parameters in each region are shown in Table 1, where x is the aluminum concentration in $Al_xGa_{1-x}As$ system. *Calcu.* in the column of the width W_i or the thickness d_i indicates to assign the larger value of the carrier diffusion length or the field distribution range after determining the field distribution as already mentioned in the last section. Another *Calcu.* in the column τ_{si} is to use Eq. (9) for the direct transition material, while longer value of $\tau_{si} = 1.0 \times 10^{-5}$ is assumed for the indirect transition material.

Regions of $i = 1$ to 6 are counted in the rate equations, but other regions of $i = 7$ to 10 need not to be counted, because these regions are made of indirect materials having no interaction with the photon characterized as $a_i = 0$ and changes of the carrier number in these regions are negligible. The two electrodes of $i = 6$ and $6'$ can be treated together as $i = 6$ in the rate equations, because these regions are electrically connected in the external current source whose stored electron number is constant.

Other assumed parameters are $\lambda_o = 8.267 \times 10^{-7}$m, $\Delta\omega = 7.00 \times 10^{13}\text{sec}^{-1}$, $n_{r0} = 3.60$, $\kappa = 1000\text{m}^{-1}$, $R_b = 0.75$, $R_f = 0.12$, $L = 3.75 \times 10^{-4}$m, $A_s = 1.16 \times 10^{-16}\text{m}^3\text{sec}^{-1}$, $9\omega\tau_{in}^2 R_{cv}^2/(4\epsilon_o n_{ro}^2\hbar) = 1.40 \times 10^{-23}\text{m}^3$, $D_c = 3.6 \times 10^{-3}\text{m}^2\text{sec}^{-1}$, and $\alpha = 2.7$, where $\alpha$is the so called line-enhancement factor which gives the ratio of (refractive index change)/(gain change) as will be introduced in Eq. (39).

Since the gain v.s. injected carrier density characteristic is not linear and the injected carrier density $n_3 (= N_3/V_3)$ in S.A. region varies in a wide range, we suppose two sets of a_3 and n_{g3} corresponding to range of $n_3 < 6.0 \times 10^{24}\text{m}^{-3}$ and $n_3 \geqq 6.0 \times 10^{24}\text{m}^{-3}$.

Important assumptions of this paper may be on the diffusion mechanisms and the carrier injection among the regions. As the diffusion between the Act. and the Adj. regions, the ambipolar diffusion is assumed with factors of

$$f_{12} = f_{21} = 1.0 \tag{30}$$

while, the electron diffusion from the S.A. to the Cu.Bl. regions and the hole diffusion from the Cu.Bl. to the S.A. regions are assumed with factors of

$$f_{34} = 0.5,\ f_{43} = 0.1\ . \tag{31}$$

Diffusions among other regions are ignored by putting $T_{ij} \to \infty$ with $f_{ij} \to 0$.

The current component I_p is assumed to be induced by the diffusion between the S.A. and the Cu.Bl. regions as

$$I_p = e(N_3/T_{34} - N_4/T_{43}) \tag{32}$$

In actual numerical calculations, the second term of N_4/T_{43} corresponding to the hole diffusion becomes much smaller than the first term of the electron diffusion because of $N_4 \ll N_3$.

The leak current I_l might be determined in principle through evaluation of the diffusion resistance in the Cl.2 region. Since such evaluation is not easy, we assumed in this paper that the leak current I_l is proportional to the total current I with a fixed ratio, for example

$$I_l = 0.4I \tag{33}$$

as a simple numerical setting.

The carrier injecting terms are written as,

$$\begin{aligned} &I_{65} = I,\ I_{53} = I_o + I_l = I - I_p \\ &I_{31} = I_o + I_p = I - I_l,\ I_{45} = I_p,\ I_{36} = I_l \end{aligned} \tag{34}$$

with

$$\begin{aligned} &k_{65} = I \\ &k_{53} = I + eN_4/T_{43},\ k_{35} = eN_3/T_{34} \\ &k_{31} = I,\ k_{13} = I_l \\ &k_{45} = eN_3/T_{34},\ k_{54} = eN_4/T_{43} \\ &k_{36} = I_l \end{aligned} \tag{35}$$

I_{36} is the leak current flows along regions $i = 3, 7, 8, 2$ and 10 to $6'$.

Corresponding fluctuated terms are

Table 1 Geometrical and material parameters.

No.	Name	Type	x	w_i [m]	d_i [m]	τ_{si} [sec]	a_i [m^3/sec]	n_{gi} [m^{-3}]	
6	Electr.	Metal							
5	Cap	p	0.50	3.0×10^{-6}	Calcu.	10×10^{-5}	0.0	0.0	
3	S. A.	p	0.00	3.0×10^{-6}	4.0×10^{-9}	Calcu.	2.50×10^{-11}	6.00×10^{24}	for $n_3 < 6.00 \times 10^{24}$
							2.76×10^{-12}	1.20×10^{24}	for $n_3 \geq 6.00 \times 10^{24}$
4	Cu.Bl.	n	0.65	Calcu.	Calcu.	10×10^{-5}	0.0	0.0	
7	Cl.1	p	0.50	3.0×10^{-6}	3.0×10^{-7}	10×10^{-5}	0.0	0.0	
8	Cl.2	p	0.50	Calcu.	3.0×10^{-7}	10×10^{-5}	0.0	0.0	
1	Act.	i	0.14	3.0×10^{-6}	4.0×10^{-8}	Calcu.	2.76×10^{-12}	1.20×10^{24}	
2	Adj.	i	0.14	Calcu.	4.0×10^{-8}	Calcu.	2.76×10^{-12}	1.20×10^{24}	
9		n	0.50	3.0×10^{-6}	Calcu.	10×10^{-5}	0.0	0.0	
10		n	0.50	Calcu.	Calcu.	10×10^{-5}	0.0	0.0	

$$-I_{53\Omega} = I_{45\Omega} = e(N_{3\Omega}/T_{34} - N_{4\Omega}/T_{43}) \tag{36}$$

All other carrier injections other than those mentioned in Eqs. (34) to (36) are put as $I_{ji} = 0$, $k_{ji} = 0$ and $I_{ji\Omega} = 0$.

As numerical calculations, we supposed three types of setting. The first one is "No Photon Recycling Current" and "No Leak Current" by putting $I_p = 0$ with $T_{34} \to \infty$ and $T_{43} \to \infty$ and $I_l = 0$. The second one is "With Photon Recycling Current" and "No Leak Current" by supposing Eq. (32) and $I_l = 0$. The third one is "With Photon Recycling Current" and "With 40% Leak Current" by supposing Eqs. (32) and (33).

5. Calculation Procedure

The first step of the numerical calculations is to analyze the field distribution. The distribution in the transverse cross-section is analyzed basing on the so called equivalent refractive index method [4]. The regions are separated into two groups of the internal regions consisting of Nos. 9, 1, 7, 3 and 5 and the external regions consisting of Nos. 10, 2, 8 and 4. The boundaries along the lateral (x) direction are ignored in each group. The refractive index n_{ri} of the i-th region is determined with the aluminum concentration x in relation of

$$n_{ri} = n_{ro} - 0.71x + 0.091x^2 . \tag{37}$$

The obtained field distribution in the internal regions is shown in Fig. 4 (a). The field is well concentrated to the Act. region and shows almost smooth distribution around the S.A, region. We evaluated the effective refractive index $n_{r.in}$ and the effective propagation loss κ_{in} from the field propagation constant along the longitudinal (z) direction.

A similar distribution is obtained in the external regions with the effective refractive index $n_{r.ex}$ and the loss κ_{ex}. Since we have not assumed any additional loss, $\kappa_{in} = \kappa_{ex} = \kappa$ is held in this paper.

The field distribution along the lateral (x) direction is analyzed with these effective parameters basically, but the change in the material parameters due to variation of the injected carrier density has to be added, because difference of $n_{r.in} - n_{r.ex}$ is not large enough.

The gain difference Δg between the internal region and the external region is given as

$$\begin{aligned}\Delta g = \frac{n_{ro}}{c}[&a_1\xi_{y1}(n_1 - n_{g1}) + a_3\xi_{y3}(n_3 - n_{g3}) \\ &- a_2\xi_{y2}(n_2 - n_{g2}) - a_4\xi_{y4}(n_4 - n_{g4})] \\ &- \kappa_{in} + \kappa_{ex}\end{aligned} \tag{38}$$

where, ξ_{yi} is the one dimensional field confinement ratio along the thickness (y) direction. The nolmalized refractive index difference Δn_r is then counted as

$$\Delta n_r = \frac{n_{r.in} - n_{r.ex}}{n_{r.ex}} - \frac{\alpha\lambda_o\Delta g}{4\pi n_{ro}} . \tag{39}$$

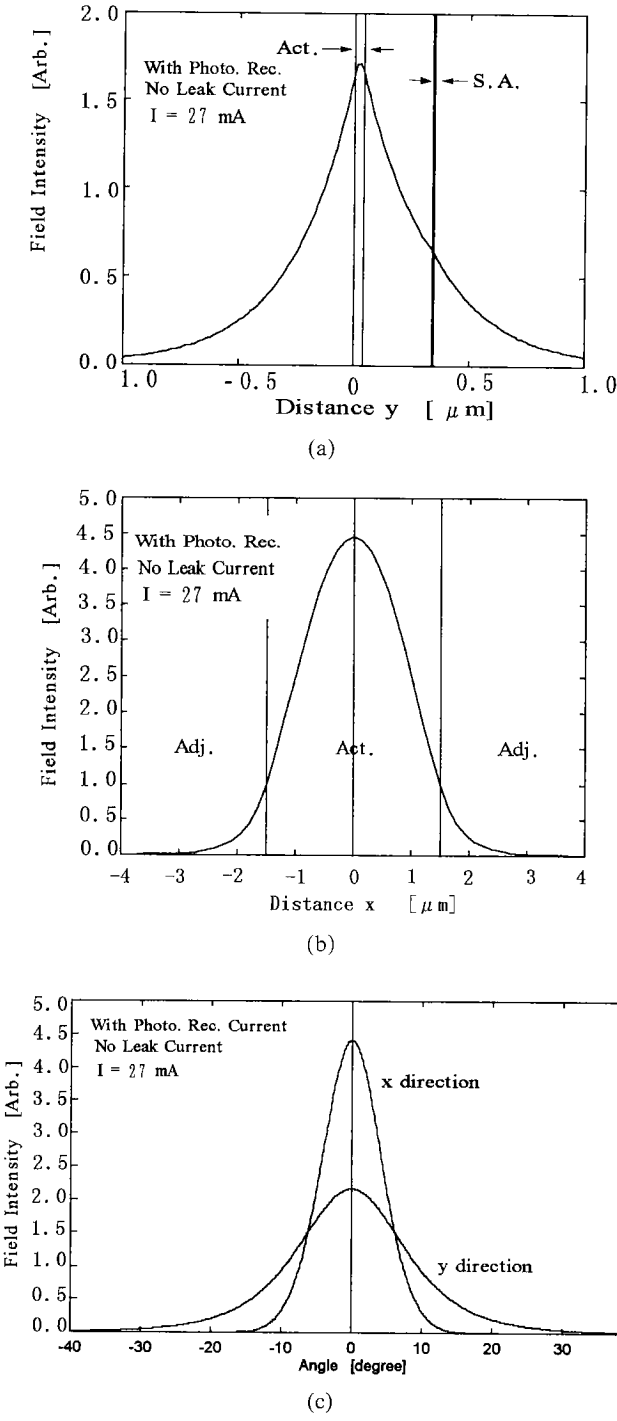

Fig. 4 Field distributions. (a) is a near-field pattern along the thickness y direction which is stable during pulsation operation, (b) is a timely averaged near-filed pattern along the lateral x direction, (c) gives far-field patterns corresponding to (a) and (b).

The field distribution along the lateral (x) direction is calculated with these two parameters of Δg and Δn_r together with the stripe width W_i [11], [12].

Actual calculation of the field distribution along the lateral (x) direction is done at each instantaneous

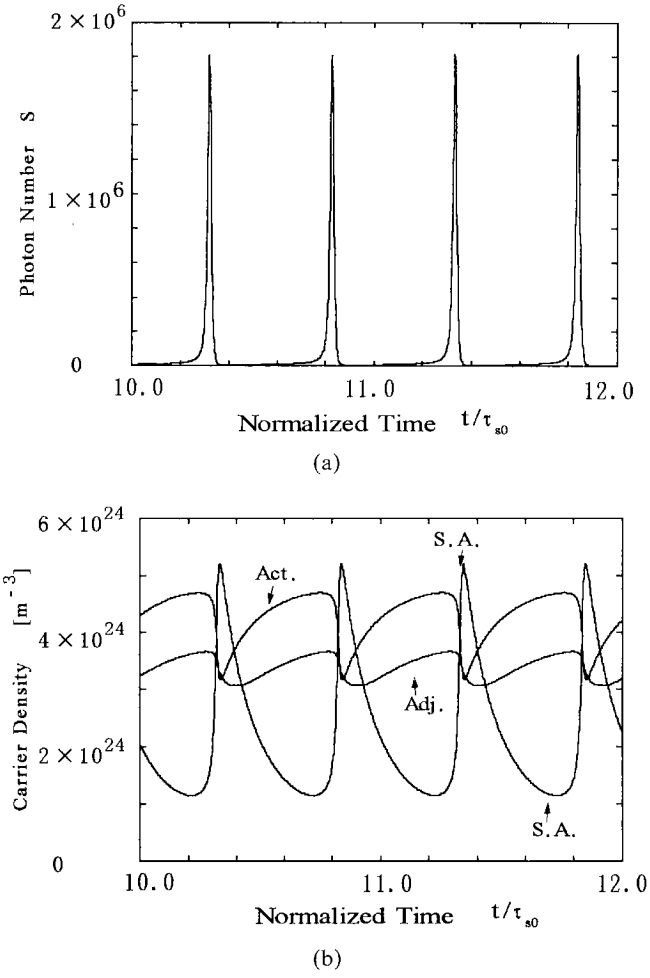

Fig. 5 Pulsing shapes of photon and carrier densities.

time under pulsing operation since the injected carrier densities varies instantaneously. An obtained example of the field distribution for timely averaged value is shown in Fig. 4 (b). Neatly stable field distribution with the so called index guiding is obtained with given parameters in the Table 1. Far field patterns corresponding to Figs. 4 (a) and (b) are shown in Fig. 4 (c).

The second step of the calculation is to determine the pulsing operation with Eqs. (24) and (25). The field distributions along the thickness (y) direction are stable and have been already fixed. Initial values of the parameters at $t = 0$ are assumed such that $n_1 = 2n_{g1}$, $n_2 = 0.3n_{g2}$, all other carrier densities are set as $n_i = 0$ and $\tau_{s1} = \tau_{s2} = \tau_{s3} = \tau_{so} = 5.0 \times 10^{-9}$ sec. The field distribution along the lateral (x) direction and other geometrical parameters are calculated with these parameters.

Then tracings of the photon number and the injected carrier numbers as well as other parameters are started up by help of the Lunge-Kutta method as shown in Fig. 5 for a given injection current I, where the time is normalized with $\tau_{so} = 5 \times 10^{-9}$ sec. The time resolution in the calculation is $\tau_{so}/1000$.

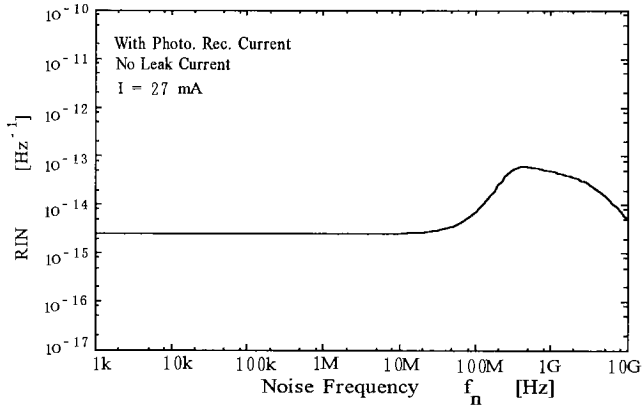

Fig. 6 Frequency characteristics of RIN.

The variation of the carrier density in the Adj. region is almost same as that in the Act. region in this example. However, variation in the S.A. region reveals a typical behavior to be the saturable absorbing region against the variation of the Act. region. The injected carrier density in other regions, such as the Cu.Bl. and the Cap, are very small and are not so varied with the time.

The calculation has to be done up to sufficiently long time, such as $t = 15\tau_{so}$, to determine whether the pulsation continues or converges to the CW operation from the damping oscillation. Several timely averaged values, such as $\overline{N_i}$, $\overline{S}$, $\overline{a_i \xi_i N_i / V_i}$ and so on, are calculated through the pulsing calculation to prepare to the noise calculation and other requirements. For example, the field distribution in the lateral (x) direction as in Figs. 4 (b) and (c) should be examined with averaged carrier densities which have the weight of the photon number as $\sum_m n_i(t_m)S(t_m) / \sum_m S(t_m)$ not with a simple average of $\sum_m n_i(t_m) / \sum_m$, because the field measurement is proportional to the field strength. Figures 4 (b) and (c) were thus obatained.

The third step of the calculation is to determine the noise level. By substituting the several timely averaged values which have been obtained during the pulsing examination into Eq. (28). Then we get the noise profile as in Fig. 6.

6. Variation of Characteristics with Injection Current or Output Power

The calculated results are shown in the series of figures from Fig. 7 to Fig. 10 with the variation of the injection current I or the timely averaged DC output power P_{out} for strength of the self-sustained pulsation which is given as the ratio of the peak power to the averaged DC power, for pulsation frequency and for the relative intensity noise (RIN).

The upper limits of the operating range in Fig. 7 indicate upper boundaries to get the self-sustained pulsa-

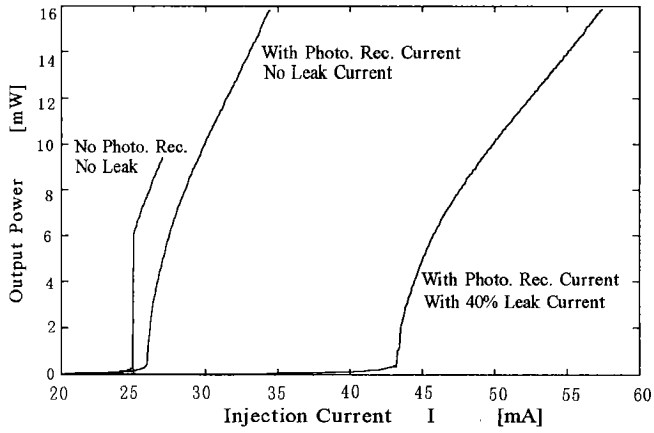

Fig. 7 Averaged DC output power vs. injection current characteristics. Upper limits of the data are determined by conditions of getting the self-sustained pulsation.

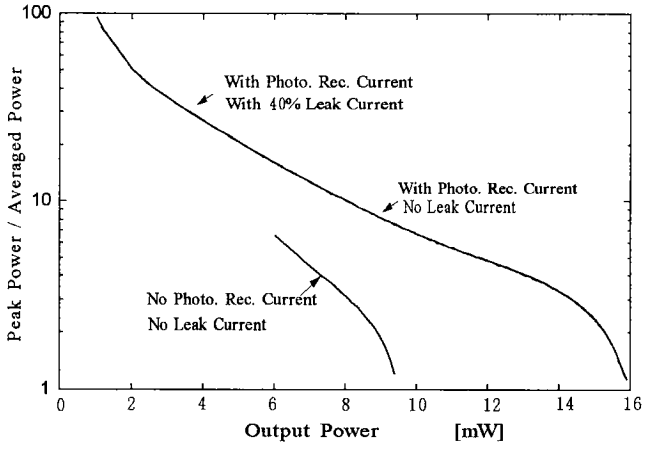

Fig. 8 Intensity of self-sustained pulsation vs. averaged DC output power characteristics. Two lines with photon recycling current are overlapped and have almost same characteristics.

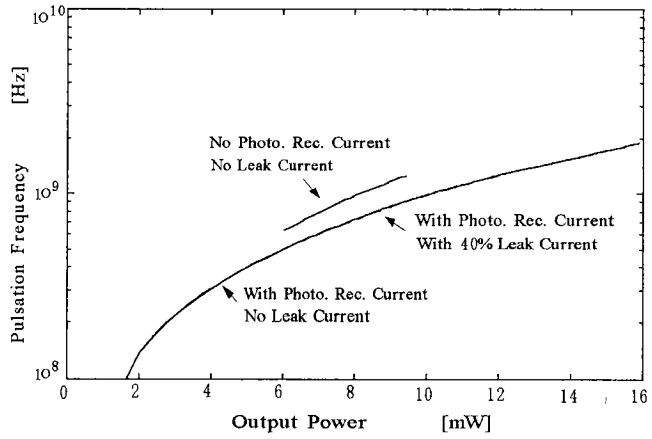

Fig. 9 Pulsation frequency vs. averaged DC output power characteristics. Two lines with photon recycling current are overlapped and have almost same characteristics.

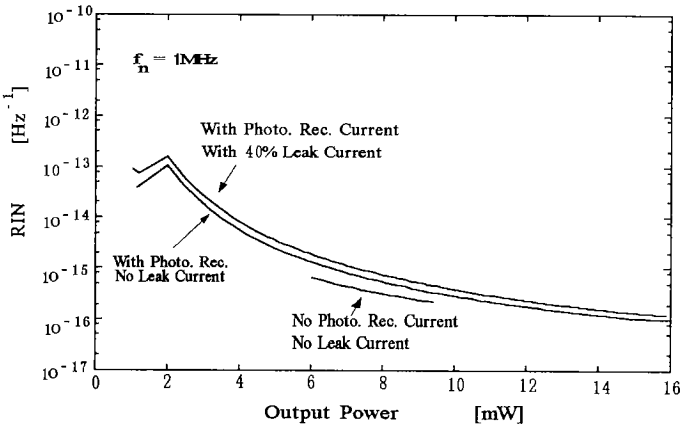

Fig. 10 RIN vs. averaged DC output power characteristics.

tion. The conventional CW operation is obtained with a higher current level than the line shown in Fig. 7. The described ranges in Figs. 8 to 10 also correspond to the operating ranges of the self-sustained pulsation.

As found in Figs. 7 to 9, the self-pulsation can be expanded to a higher power level with a higher pulsation intensity by help of the photon recycling effect as was expected in the discussion in Sect. 2. However, the noise is enhanced by the photon recycling effect as found in Fig. 10.

The photon recycling effect in our model slightly increases the threshold current as shown in Fig. 7. Although the generated holes by the optical absorption in the S.A. region is re-injected into the Act. region, the generated electrons diffuse into the Cu.Bl. regions and re-combine with other holes in the Cu.Bl. regions or the p-type Cap region. This effect is equivalent to increase the optical loss.

The leak current does not directly affect the self-sustained pulsation as indicated in Figs. 8 and 9, but simply pulls the characteristics toward a higher current level as sown in Fig. 7. However, the noise is raised by this leak current as in Fig. 10 especially for the lower power operation.

7. Conclusions

The quantum (intensity) noise in the self-sustained pulsation lasers is theoretically examined by taking into account additional current components due to the photon recycling effect and the leak current. The obtained results are:

1. When generated electrons in the p-type saturable absorbing (S.A.) region can diffuse into the n-type current blocking (Cu.Bl.) layer, generated holes in the S.A. region are injected to the active (Act.) region resulting in the photon recycling effect.

2. This type of photon recycling can enhance not only the self-sustained pulsation but also the quantum noise especially at the operation with a low output power.

3. The ridge-type stripe structure with current blocking regions, which is typically applied for the self-sustained pulsation laser, tends to give a leak current flowing along the cladding (Cl.2) layer and making recombination in the adjoining (Adj.) regions at far positions from the active (Act.) region.

4. This type of leak current raises not only the threshold current level but also the quantum noise especially at the operation with a low output power.

As deduced from these results, the existence of the leak current is not absolutely suitable for the performance of the laser. The saturable absorbing (S.A.) region should be designed basing on the alternative selection of either stronger self-pulsation or lower quantum noise.

In this paper, we did not include analysis for operation when the laser suffers an optical feedback from a connecting device such as the optical disk. Analysis of this problem will be given in near future by the author by extending the analytical method of this paper.

Acknowledgment

This research is supported by Sharp Co. Ltd., Sony Co. Ltd., Mitsubishi Electric Co. Ltd. and Fujitsu Lab. Co. Ltd.

References

[1] S. Matsui, H. Takiguchi, H. Hayashi, S. Yamamoto, S. Yano, and T. Hijikata, "Suppression of feedback-induced noise in short-cavity V-channeled substrate inner stripe lasers with self-oscillation," Appl. Phys. Lett., vol.43, no.3, pp.219–221, 1983.
[2] S. Yamashita, A. Ohishi, T. Kajimura, M. Inoue, and Y. Fukui, "Low-noise AlGaAs lasers grown by organometallic vapor phase epitaxy," IEEE J. Quantum Electron., vol.25, no.6, pp.1483–1488, 1989.
[3] M. Yamada, "Theoretical analysis of noise-reduction effect in semiconductor lasers with help of self-sustained pulsation phenomena," J. Appl. Phys., vol.79, no.1, pp.61–71, 1996.
[4] M. Yamada, "A theoretical analysis of self-sustained pulsation phenomena in narrow-stripe semiconductor lasers," IEEE J. Quantum Electron., vol.29, no.5, pp.1330–1336, 1993.
[5] T. Takayama, O. Imafuji, M. Yuri, H. Naito, M. Kume, A. Yoshikawa, and K. Itoh, "800 mW peak-power self-sustained pulsation GaAlAs laser diodes," IEEE J. Selected Topics in Quantum Electron., vol.1, no.2, pp.562–568, 1995.
[6] T. Goto, N. Hayashi, A. Ibaraki, D. Ide, K. Furusawa, K. Yodoshi, and T. Niina, "Low-noise, high-power GaAlAs laser diode with a saturable absorbing layer," MOC'95, Technical Digest, pp.278–281, 1995.
[7] H. Adachi, I. Kidoguchi, T. Fukuhisa, K. Tanaka, M. Amannoh, and A. Takamori, "Reduction of aspect ratio in 650-nm band self-sustained-pulsing lasers with saturable-absorbing layer," Jpn. J. Appl. Physics, vol.36, Part 1, no.3B, pp.1876–1879, 1997.
[8] H. Haug, "Quantum-mechanical rate equations for semiconductor lasers," Phys., Rev., vol.184, no.2, pp.338–348, 1969.
[9] T.L. Paoli, "Noise characteristics of stripe-geometry double-hetero-structure junction lasers operating continuously—I. Intensity noise at room temperature," IEEE J. Quantum Electron., vol.QE-11, no.4, pp.276–283, 1975.
[10] M. Yamada, "Variation of intensity noise and frequency noise with the spontaneous emission factor in semiconductor lasers," IEEE J. Quantum Electron., vol.30, no.7, pp.1511–1519, 1994.
[11] Y. Suematsu and M. Yamada, "Oscillation-mode and mode-control in semiconductor lasers with stripe-geometry," IECE Trans., vol.57-c, no.11, pp.434–440, 1974.
[12] M. Yamada, "Transverse and longitudinal mode control in semiconductor injection lasers," IEEE J. Quantum Electron., vol.QE-19, no.9, pp.1365–1380, 1983.

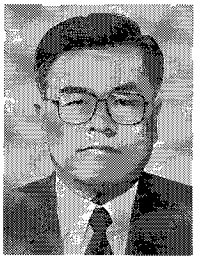

Minoru Yamada was born in Yamanashi, on January 26, 1949. He received the B.S. degree in electrical engineering from Kanazawa University, Kanazawa in 1971, and M.S. and Ph.D. degrees in electronics engineering from the Tokyo Institute of Technology, Tokyo in 1973 and 1976, respectively. He joined Kanazawa University in 1976, and is presently a Professor. From 1982 to 1983, he was a Visiting Scientist at Bell Laboratories, Holmdel, NJ, U.S.A. He is currently working in semiconductor injection laser. Dr.Yamada received the Yonezawa Memorial Prize in 1975, the Paper Award in 1976, and the Achievement Award in 1978 from the IECE of Japan.